ELSEVIER

Journal of Power Sources 104 (2002) 140–147

JOURNAL OF POWER SOURCES

www.elsevier.com/locate/jpowsour

Studies of the effects of the reformer in an internal-reforming molten carbonate fuel cell by mathematical modeling

Hong-Kyu Park[a], Ye-Ro Lee[a], Mi-Hyun Kim[a], Gui-Yung Chung[a,*], Suk-Woo Nam[b], Seong-Ahn Hong[b], Tae-Hoon Lim[b], Hee-Chun Lim[c]

[a]*Department of Chemical Engineering, Hong-ik University, 72-1 Sangsudong Mapoku, Seoul 121-791, South Korea*
[b]*Battery and Fuel Cell Research Center, KIST, Seoul, South Korea*
[c]*KEPRI, Seoul, South Korea*

Received 4 June 2001; accepted 20 August 2001

Abstract

The effects of the reformer in an internal-reforming molten carbonate fuel cell (IR-MCFC) are studied by mathematical modeling. Temperature distributions, conversion of methane and compositions of gases are analyzed through mathematical modeling of the reformer and the cell. In the reformer, the methane-reforming reaction and the water-gas shift reaction occur simultaneously and the conversion of methane to hydrogen, calculated including the thermodynamic equilibrium of the reaction, reaches 99%. Additionally, the endothermic-reforming reaction contributes to a uniform temperature distribution. The voltage and the power of the IR-MCFC are similar to those of an external-reforming molten carbonate fuel cell (ER-MCFC), when the compositions at the inlet of the ER-MCFC are set as those at the outlet of the reformer in IR-MCFC. As the molar ratio of methane to water-gas decreases at a fixed total flow rate, the working voltage decreases.
© 2002 Elsevier Science B.V. All rights reserved.

Keywords: MCFC; Reformer; Methane-reforming reaction; Water-gas shift reaction

1. Introduction

With regulation of exhaust emissions and increase in the use of electrical energy, investments in fuel cells are increasing. Fuel cells are of interest because they do not produce nitric oxide which can be a source of air pollution, have excellent efficiency in converting chemical energy into electrical energy, and can be scaled-up inexpensively. Molten carbonate fuel cells (MCFCs) do have demerits, however, in that they work at a high temperature and the molten carbonate is very corrosive.

The temperature distribution in fuel cells becomes non-uniform due to the heat produced by the electrochemical reaction, the ion transfer in an electrolyte plate, and the resistance to electron movement in the electrodes. This produces a non-uniform electrochemical reaction, thermal stress, vaporization of electrolyte, and corrosion of materials. As a result, the performance of fuel cells decreases rapidly. Thus, it is important to obtain a uniform temperature distribution without locally heated areas [1].

An electrochemical reaction and a methane-reforming reaction occur simultaneously in the internal-reforming MCFC. Hence, the thermal efficiency of the device increases and the system becomes simple, because the heat of generation from the electrochemical reaction can be used directly for the endothermic-reforming reaction without being removed to the surroundings [2].

In the internal-reforming MCFC, H_2 and CO are formed by the water-gas shift reaction ($CO + H_2O \leftrightarrow CO_2 + H_2$) and the methane-reforming reaction ($CH_4 + H_2O \leftrightarrow CO + 3H_2$). Furthermore, the fractions of reactants and products are determined by the rates of these reactions, as well as by the thermodynamic equilibrium [3]. Hence, it is necessary to consider the thermodynamic equilibrium carefully. The cell temperature, 650 °C, is not sufficiently high to reach equilibrium for the methane-reforming reaction. Therefore, the fraction of methane reformed due to the thermodynamic equilibrium is only 85% [4]. Nevertheless, the produced hydrogen and carbon monoxide reach the equilibrium of the water-gas shift reaction immediately in the cell. Hence, the equilibrium moves in the direction of producing hydrogen. So methane is consumed and hydrogen is produced by the methane-reforming reaction and the water-gas shift reaction.

* Corresponding author. Tel.: +82-2-320-1681; fax: +82-2-320-1191.
E-mail address: gychung@wow.hongik.ac.kr (G.-Y. Chung).

0378-7753/02/$ – see front matter © 2002 Elsevier Science B.V. All rights reserved.
PII: S0378-7753(01)00912-0

Nomenclature

B	thickness (cm)
C_p	heat capacity (J/g mol K)
d_{ct}	diameter of a cylindrical catalyst (cm)
d_m	thickness of metal part in reformer (cm)
E	open circuit voltage (V)
f_i	material volume per reformer volume
F	Faraday's constant (96,501 C/eq.) (26.8 Ah/g mol)
h	heat transfer coefficient (J/cm^2 h K)
H_{ct}	length of catalyst (cm)
I	current density (mA/cm^2)
k	thermal conductivity (J/cm h K)
k_r	methane-reforming reaction rate constant (g mol/atm h)
K_s	equilibrium constant of the water-gas shift reaction
L	length of the fuel cell (cm)
m	molar flow rate (g mol/cm h)
n_i	mole flux of fuel gas (g mol/h)
N_c	number of catalyst in Δx
p	pressure (bar)
Q	heat of generation per unit cell area (J/cm^2)
R	gas constant (82.06 cm^3 atm/g mol K) (8.314 J/g mol K)
R_{ohm}	ohmic cell resistance (Ω)
R_r	reforming reaction rate (g mol/h)
R_s	rate of water-gas shift reaction (g mol/h)
T	temperature (K)
V	cell operating potential (V)
W	width of the fuel cell (cm)
X_i	mole fraction of the ith gas component
Z	effective cell resistance (Ω/cm^2)

Greek symbols

η_a	anodic overpotential (V)
η_c	cathodic overpotential (V)

Subscripts

a	anode
c	cathode
ct	catalyst
e	electrode–electrolyte
i	value at the inlet of the gas
m	metal
mg	methane gas
re	reformer
sg	surrounding gas
up	upper plate
us	upper separator

Superscript

0	value at the entrance

In this paper, mathematical modeling of a 100-cm^2 fuel cell is under taken. The temperature distribution, voltage distribution, and performance of an internal-reforming fuel cell at a constant current density are calculated and compared with those of an external-reforming fuel cell.

2. Theory

A schematic diagram of the internal-reforming MCFC used in the mathematical modeling is shown in Fig. 1. The reforming section is composed of an upper plate, a catalyst layer, and an upper separator. In the catalyst layer, cylindrical catalysts of radius, r, and length, b, are arranged in zigzag along the direction of the gas flow. In our mathematical modeling, however, it is assumed that catalyst, metal and the fuel gas path are distributed uniformly in the catalyst layer with proportions 0.22, 0.04 and 0.74, respectively.

Reactant gases flow in parallel with the axes of the cylindrical catalysts with a velocity v per unit cross-sectional area. A Ni-Mo catalyst was used. Diffusion into the pores of the cylindrical catalysts is ignored. Fuel gas, which passes through the catalyst layer of the fuel cell, makes a U-turn and is used as the anode gas.

Gases flow in a cross type, i.e. anode gas flows in the x-direction and cathode gas in the y-direction. The paths of anode and cathode gases form a channel. The channels in the gas paths are neglected, however, and the paths are assumed

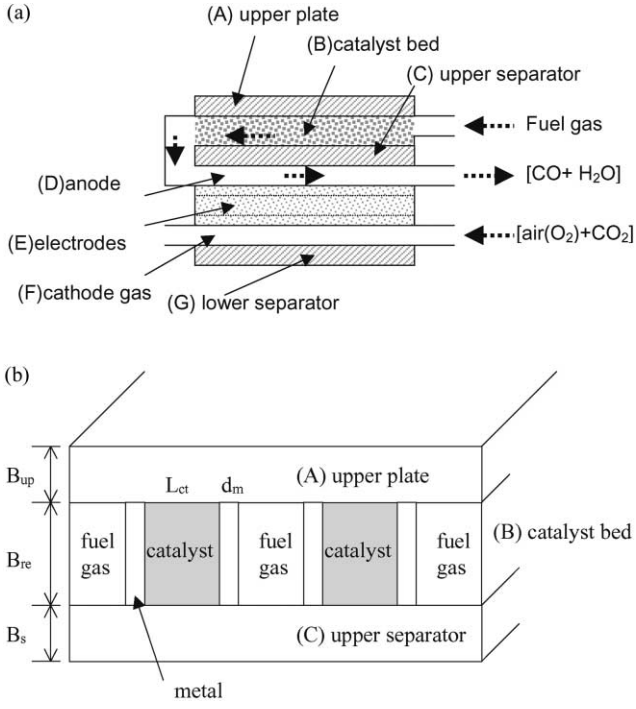

Fig. 1. Schematic diagram of (a) internal-reforming MCFC; (b) methane reformer. (A) Upper plate, (B) catalyst bed, (C) upper separator, (D) anode gas channel, (E) electrode–electrolyte plate, (F) cathode gas channel and (G) lower separator.

to be rectangular. Additionally, since the thicknesses of the separators, the paths of gases, and the electrode–electrolyte plate are small compared to the lengths and the widths, temperature and concentration gradients in the direction of depth are not considered. The fuel cell is assumed to operate at a steady state and the surroundings are assumed to be adiabatic. Radiation energy absorbed by gases between a separator plate and an electrode–electrolyte plate is also neglected [5].

The rate of the methane-reforming reaction (R_r) and the rate of the water-gas shift reaction (R_s) from an equilibrium equation can be obtained from the following equations, respectively [6,7]:

$$-R_r = k_r p_{CH_4} \tag{1}$$

$$K_s = \frac{(nX_{CO_2} - f_{mg}R_s)(nX_{H_2} + 3R_r - f_{mg}R_s)}{(nX_{CO} + R_r + f_{mg}R_s)(nX_{H_2O} + R_r + f_{mg}R_s)} \tag{2}$$

Here, k_r (g mol/atm h) is the rate constant of the methane-reforming reaction and is 0.0128 at 923 K. n is the molar flux of entering gas. Using R_r and R_s calculated from Eqs. (1) and (2), the mass balance equation about the methane-reforming section is obtained as follows:

$$n_{in}x_{k,in} - n_{out}x_{k,out} + R_r + f_{mg}R_s = 0 \tag{3}$$

Here, the subscript k represents each component of the fuel gases, i.e. methane, hydrogen, carbon dioxide, steam, and carbon monoxide. As shown in Fig. 1, methane and steam are supplied as a fuel gas into the catalyst layer and produce carbon monoxide and hydrogen. Then, carbon monoxide and hydrogen are introduced as an anode gas. The term f_{mg} in Eq. (3) is the volume fraction of fuel gas in the reforming section.

The same mass-balance equations of anode gas and cathode gas are used in [5]. The current density, I, and the voltage, V, of cells has the following relationship [8]:

$$V = (V_{cN} - V_{aN}) - IR_{ohm} + \eta_c - \eta_a \tag{4}$$

Here, the voltages of the cathode and the anode, V_{cN} and V_{aN}, are obtained from the Nernst equation and the overpotentials η_c and η_a are obtained from multiplication of current density and polar resistance (Z_c and Z_a) [8]. The values of the polar resistances are calculated using the functions for the gas compositions and the reaction temperature proposed by Selman [9] and the value of ohmic cell resistance, R_{ohm}, is calculated using a function of temperature [10]. By inserting the equations for V_{cN}, V_{aN}, η_c, η_a and R_{ohm}, in Eq. (4), the following equation can be obtained and the value of the voltage can be obtained:

$$V = (V_a^0 - V_c^0) - \frac{RT}{2F}\ln\left(\frac{X_{cC}X_O^{1/2}X_H}{X_wX_{aC}}\right) - IZ \tag{5}$$

Here, X_{cC} and X_{aC} are the mole fractions of CO_2 in the cathode gas and anode gas, respectively. X_w is the mole fraction of H_2O in the anode gas.

Energy balance equations for the methane-reforming section are as follows. Upper plate (A in Fig. 1):

$$\frac{\partial^2 T_{up}}{\partial x^2} + \frac{\partial^2 T_{up}}{\partial y^2} = \frac{h_{sg,up}}{B_{up}k_{up}}(T_{up} - T_{sg}) + \frac{f_{mg}h_{mg,up}}{B_{up}k_{up}}(T_{up} - T_{mg}) + \frac{2f_m}{B_{up}^2}(T_{up} - T_m) + \frac{2f_{ct}}{B_{up}^2}(T_{up} - T_{ct}) + \frac{f_{mg}h_{us,up}}{B_{up}k_{up}}(T_{up} - T_{us}) \tag{6}$$

The boundary conditions are as follows:

$$\text{at } x = 0 \quad \text{and} \quad x = L, \text{for all } y : \frac{\partial T_{up}}{\partial x} = 0 \tag{7}$$

$$\text{at all } x, y = 0 \quad \text{and} \quad y = W : \frac{\partial T_{up}}{\partial y} = 0 \tag{8}$$

where h (J/cm^2 h K) is a heat transfer coefficient; k (J/cm h K), a thermal conductivity; f_{mg} and f_m are volume fractions of gases and metal parts in the reforming section, respectively. In the energy balance for the upper plate (Eq. (6)), the terms on the left-hand side represent the conductive heat transfer, and the terms on the right-hand side are the convective heat transfer with surrounding gases and methane gas, the conductive heat transfer with metals and catalysts, and the radiation heat transfer with the separator.

For methane gas in the catalyst layer (B in Fig. 1):

$$\frac{\partial(m_{mg}C_pT_{mg})}{\partial x} = h_{up,mg}(T_{up} - T_{mg}) + h_{us,mg}(T_{us} - T_{mg}) + B_{re}\sum G_iC_pT_{mg} + \frac{N_c\pi d_{ct}L_{ct}h_{ct,mg}(T_{ct} - T_{mg})}{W\Delta x f_{mg}} + \frac{2N_cL_mB_{re}h_{m,mg}(T_m - T_{mg})}{W\Delta x f_{mg}} + \frac{Q_r + Q_s}{W\Delta x f_{mg}} \tag{9}$$

Boundary condition:

$$\text{at } x = 0, \text{ for all } y : T_{mg} = T_i \tag{10}$$

where N_c, d_{ct} and L_{ct} are the number of catalyst in Δx, the diameter and the length of the cylindrical catalysts, respectively. Q_r and Q_s are the heats of the methane-reforming reaction and the water-gas shift reaction.

Metal part in the catalyst layer (B in Fig. 1):

$$\frac{4N_cL_mB_{re}k_m(T_{ct} - T_m)}{d_m} + \frac{4N_cL_md_mk_m(T_{us} - T_m)}{B_{re}} \times 2N_cL_mB_{re}h_{mg,m}(T_{mg} - T_m) + \frac{4N_cL_md_mk_m(T_{up} - T_m)}{B_{re}} = 0 \tag{11}$$

Catalyst part in the catalyst layer (B in Fig. 1):

$$\frac{4N_cL_mB_{re}k_{ct}(T_m - T_{ct})}{L_{ct}} + \frac{4N_cL_md_mk_{ct}(T_{us} - T_{ct})}{B_{re}} + \frac{2N_cL_md_mk_{ct}(T_{up} - T_{ct})}{B_{re}} + N_c\pi d_{ct}h_{mg,ct}(T_{mg} - T_{ct}) = 0 \quad (12)$$

Upper separator (C in Fig. 1):

$$\frac{\partial^2 T_{us}}{\partial x^2} + \frac{\partial^2 T_{us}}{\partial y^2} = \frac{f_{mg}h_{mg,us}}{B_sk_{us}}(T_{us} - T_{mg}) + \frac{f_{mg}h_{up,us}}{B_sk_{us}}(T_{us} - T_{up}) + \frac{2f_m}{B_s^2}(T_{us} - T_m) + \frac{2f_c}{B_s^2}(T_{us} - T_{ct}) + \frac{h_{re,s}}{B_sk_{us}}(T_{us} - T_e) + \frac{h_{sg}}{B_sk_{us}}(T_{us} - T_g) \quad (13)$$

where d_m is the thickness of the metal part, as shown in Fig. 1.

For the cell section, the previously used energy balance equations are applied [1]. The heat of electrochemical reaction can be calculated as follows [7]:

$$q_e = I\left(\frac{-T\Delta S}{2F} + (E - V)\right) = I\left(-\frac{\Delta H_e}{2F + V}\right) \quad (14)$$

where S (J/g mol K) is the entropy change due to the reaction and H_e (J/g mol) the heat of generation by the electrochemical reaction calculated as a function of temperature, T (K) [11].

$$\Delta H_e = -57,018 - 2.738T + (0.474 \times 10^{-3})T^2 + (2.637 \times 10^{-7})T^3 \quad (15)$$

Because both the methane-reforming reaction and the water-gas shift reaction occur simultaneously in the reformer, the heats of these reactions must be calculated. The amount of endothermic heat from the methane-reforming reaction is obtained as follows:

$$Q_r = \Delta n_{CH_4}\Delta H_r \quad (16)$$

where Δn_{CH_4} (g mol/h) is the number of moles of methane consumed and ΔH_r (J/g mol) the endothermic heat calculated from the following relationship [11]:

$$\Delta H_r = 190,265 + 8.314\left(7.951T - 4.354 \times 4.354^{-3}T^2 - 3.027 \times 10^{-6}T^3 - \frac{0.097 \times 10^5}{T}\right) \quad (17)$$

The amount of exothermic heat from the water-gas shift reaction is obtained from

$$Q_s = \Delta n_{CO}\Delta H_s \quad (18)$$

where Δn_{CO} (g mol/h) is the number of moles of carbon monoxide consumed by the water-gas shift reaction and ΔH_s (J/g mol) the exothermic heat of the water-gas shift reaction [11], i.e.

$$\Delta H_s = -9932.5 - 0.515T + (3.117 \times 10^{-3})T^2 - (1.05 \times 10^{-6})T^3 \quad (19)$$

Table 1
Dimensions of internal-reforming MCFC used in mathematical modeling

Cell	Length (L) (cm)	10
	Width (W) (cm)	10
	Thickness (cm)	
	Upper separator (B_{us})	0.23
	Gas channel (B_g)	0.2
	Anode electrode (B_{ea})	0.07
	Electrolyte plate (B_{em})	0.1
	Cathode electrode (B_{ec})	0.06
Reformer	Thickness (cm)	
	Upper plate (B_{up})	0.23
	Catalyst bed (B_{re})	0.12
	Catalyst	
	Diameter (d_{ct}) (cm)	0.12
	Length (L_{ct}) (cm)	0.5
	Number (N)	462

Table 2
Flow rate and composition of fuel gas

	Flow rate (mol/h)	Composition	
Fuel gas	1	CH_4	0.33
		H_2O	0.67

The variables used in the modeling are listed in Tables 1 and 2. The area of the electrode is 100 cm^2 and all calculations are made at a constant current density of 150 mA/cm^2. The temperature of the separator is 923 K, and the temperature of the entering fuel gas and that of the entering cathode gas are both fixed at 813 K.

Equations of mass and energy balances are calculated by the finite difference method. The operating voltage, temperature distribution, and the power are calculated from the modeling of the fuel cell at a steady state.

3. Results and discussion

The temperature distribution, the cell voltage and the performance of the cell are predicted by mathematical modeling of an internal-reforming 100-cm^2 unit cell at a constant current density. The conversion and composition of the gases are calculated. Additionally, changes of voltage and power with current density are also determined. The composition and temperature distribution are studied in order to evaluate the influence of the reformer on the performance of the cell. In addition, the calculated results are compared with those for an external-reforming unit cell of the same area.

3.1. Temperature distribution and cell voltage

The temperature distribution in the unit cell at a constant current density is calculated. The temperature distribution of the fuel gas is shown in Fig. 2. Since the injection

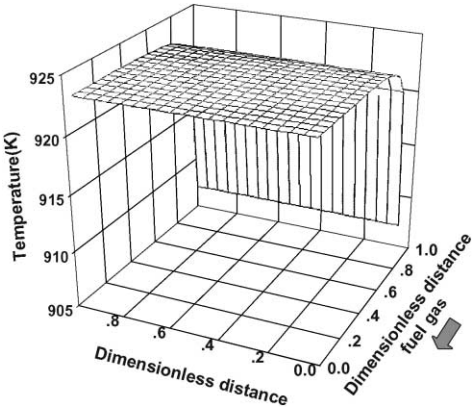

Fig. 2. Three-dimensional graph of temperature distribution of fuel gas in reformer section, (B) in Fig. 1(b), with reforming reaction and water-gas shift reaction at 150 mA/cm^2.

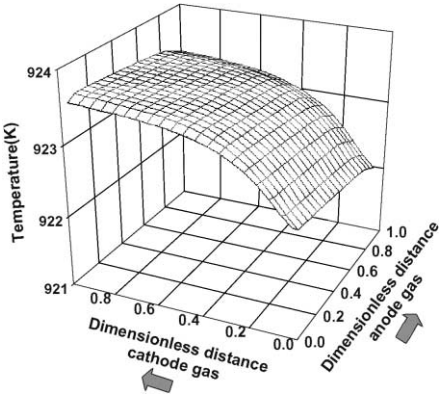

Fig. 3. Three-dimensional graph of temperature distribution of anode gas which comes from reformer section, (D) in Fig. 1(a), at 150 mA/cm^2.

temperature of the fuel gas is 813 K, the temperature of the fuel gas increases rapidly at the entrance of the cell and then becomes stable along the gas flow. Since the upper plate of the reformer is in contact with the fuel gas, its temperature increases along the direction of the fuel gas.

As the temperature of the fuel gas increases at the entrance, the reforming reaction and the water-gas shift reaction are activated together. The temperature gradient is reduced along the direction of the gas flow due to the heat of the endothermic methane-reforming reaction and the heat of the exothermic water-gas shift reaction. The heat for an endothermic reaction is supplied by the exothermic reaction. The temperature distributions become even because heat from the endothermic methane-reforming reaction is more than that from the exothermic water-gas shift reaction.

The temperature distribution of the anode gas, which is injected after passing through the reformer, is presented in Fig. 3. The water-gas shift reaction occurs in the anode gas. Since the cell is a cross-flow type, the temperature of the anode gas increases in the direction of the cathode gas flow. It decreases in the direction of the anode gas, however, because of the low temperature of the fuel gas in the reformer.

The temperature distribution of the electrode–electrolyte plate is shown in Fig. 4. It is influenced by the anode and the cathode gases and varies in the direction of the cathode gas. The temperature distribution of the electrode–electrolyte plate changes under the influence of the cathode gas. The temperature distribution is quite even in the direction of the anode gas.

The temperature distribution of the electrode–electrolyte plate is compared in Fig. 5 for MCFCs with and without internal reformers. There is little difference in the distribution in the direction of the cathode gas flow, as shown in Fig. 5(b). As shown in Fig. 5(a), however, the temperature

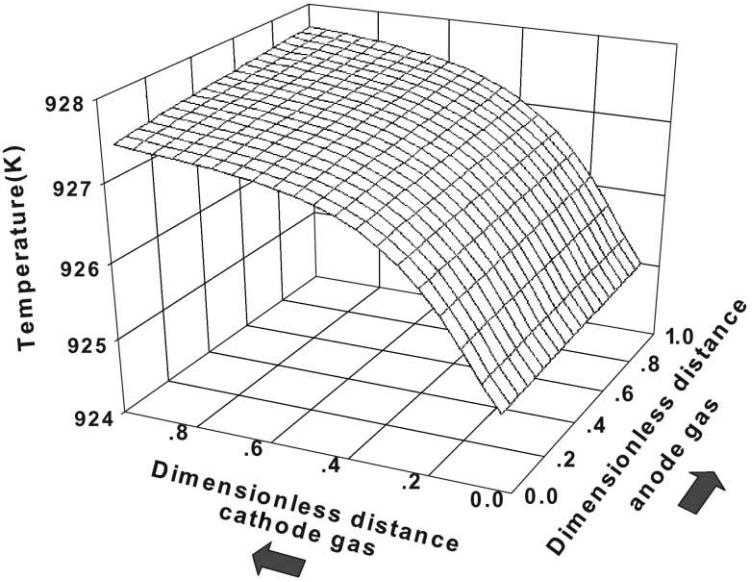

Fig. 4. Three-dimensional graph of temperature distribution of electrode–electrolyte plate, (E) in Fig. 1(a), at 150 mA/cm^2.

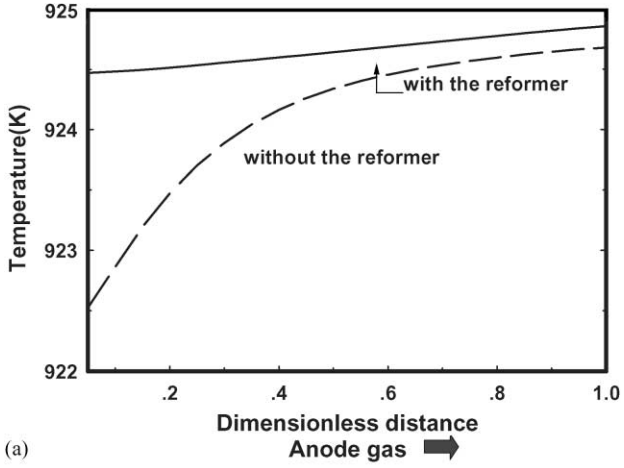

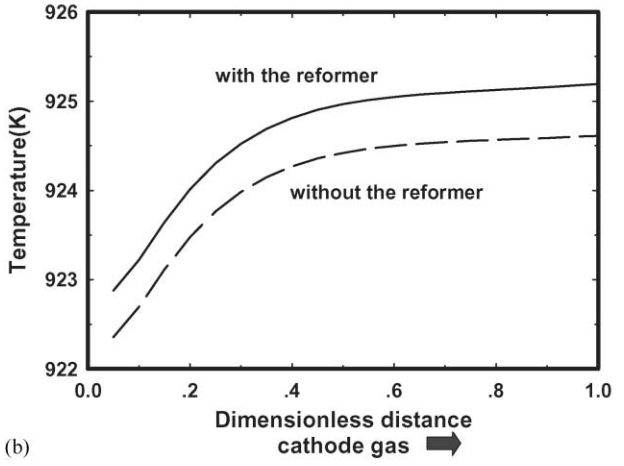

Fig. 5. Temperature distribution of electrode–electrolyte plate along direction of (a) anode gas and (b) cathode gas.

distribution in the direction of the anode gas flow become uneven due to the internal reformer. This is because, the heat from the electrochemical reaction is consumed by the methane-reforming reaction in the reformer.

3.2. Conversion of methane

The main component of the fuel gas is methane which changes into hydrogen in the reforming section. Here, there are two reactions of fuel gas, namely, the endothermic methane reaction and the exothermic water-gas shift reaction. These two reactions affect cell performance and temperature distribution. Additionally, hydrogen produced by the methane-reforming reaction is used as the anode gas. Thus, the effects of the methane-reforming reaction are analyzed.

The conversion of methane and composition of each component in the direction of the gas flow are shown in Figs. 6 and 7, respectively. The methane-reforming reaction depends on the concentration and temperature. Hence, due to the rapid rise of temperature at the entrance (Fig. 5), the methane conversion becomes 0.4 rapidly at the entrance and

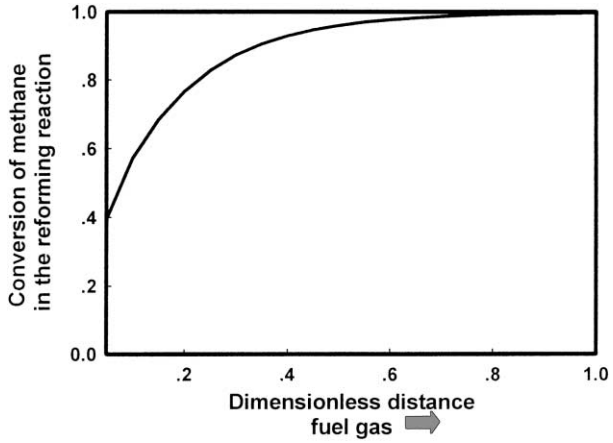

Fig. 6. Changes of conversion of fuel gas in reformer.

then rises gradually to 1 in the reforming reaction and the shift reaction while the fuel gas passes through the reformer, as shown in Fig. 6.

At the entrance of the reformer, the concentration of methane is very high and the reaction in the catalyst is very active. As the amount of methane decreases in the direction of the fuel gas, it decreases gradually. Hence, as shown in Fig. 7, the amounts of H_2O and methane decrease and the amounts of hydrogen and carbon monoxide increase. The amount of hydrogen increases by a factor of three compared with the decrease in the amount of methane. Hydrogen produced in the reformer is used as a fuel gas. The total flow rate of the fuel gas in the reformer increases as the reactions proceed. The conversion of methane in the reformer is more than 99%.

The variation in average cell voltage with current density at different ratios of fuel gas, CH_4:H_2O, is shown in Fig. 8. The current density is held constant. The voltage and power at 105 mA/cm^2 are found to be 1.05 V and 15.75 W, respectively. The compositions of the entering gas change, but the

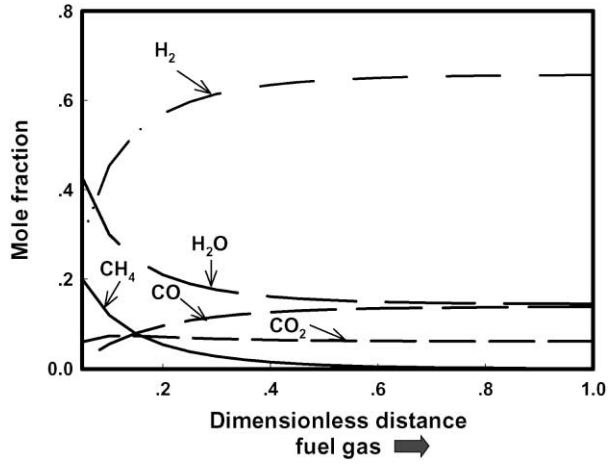

Fig. 7. Changes in mole fraction of each component in fuel gas at 150 mA/cm^2.

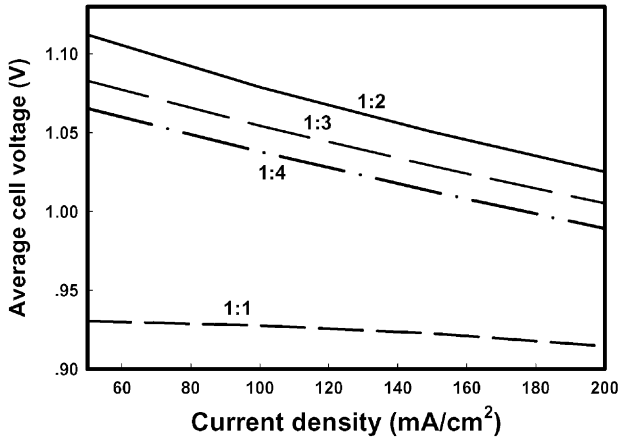

Fig. 8. Changes of cell voltage with current density at different fuel gas ratios, CH_4:H_2O.

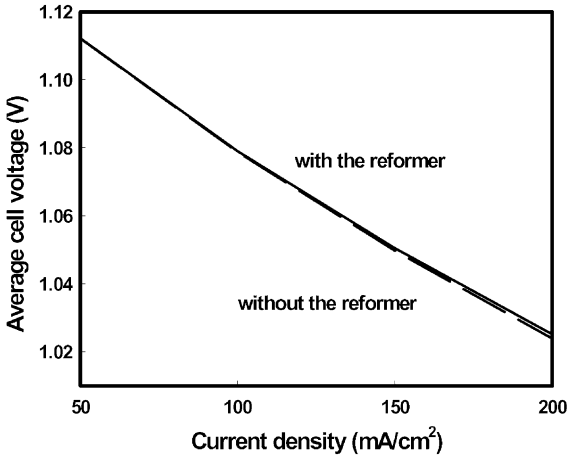

Fig. 10. Changes of average cell voltage with current density with and without reformer.

entering total flow rate is fixed. The best performance of the cell is obtained at a ratio of CH_4:H_2O = 1:2. A decrease in the ratio at a fixed total flow rate means the amount of CH_4 decreases. Hence, the amount of hydrogen from the methane-reforming reaction decreases. As the fraction of hydrogen in the fuel gas entering into the anode increases, the working voltage tends to increase. The working voltage is small at CH_4:H_2O = 1:1. This is because, there is remaining methane from the reformer, the produced hydrogen is small and the temperature becomes low. As a result, the rate of the electrochemical reaction decreases, the resistance to the movement of ions increases, and the electrode resistance of the cell increases. Additionally, the power of the cell increases with increase of hydrogen fraction, since the power is proportional to the amount of consumed hydrogen. The calculated voltages at a constant current density of 150 mA/cm^2 are given in Fig. 9. There is a difference of 0.1 V in the whole cell.

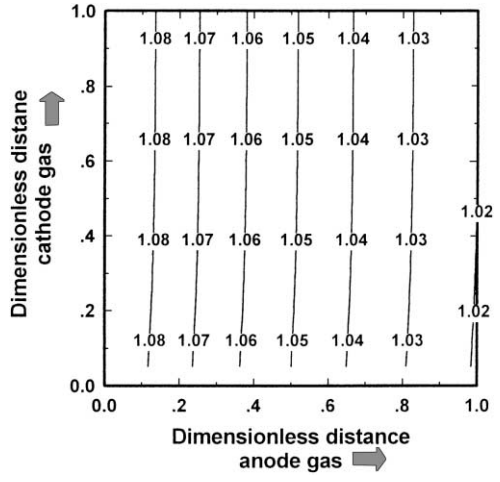

Fig. 9. Contour graph of cell voltage distribution at constant current density of 150 mA/cm^2.

3.3. Effect of current density on cell performances

The working voltage and power in internal- and external-reforming MCFCs at each current density have been calculated. Changes in the working voltage with current density are compared in Fig. 10. In this comparison, conditions such as the flow rate and composition of the entering anode gas in the external-reforming fuel cell are matched with those of the exiting gas from the reformer in the internal-reforming fuel cell. As shown in Fig. 10, the voltage depends almost linearly on the average current density. This is because the voltage decreases due to the ohmic resistance of the electrolyte. Voltages and current densities in the internal-reforming fuel cell are slightly higher than those in the external-reforming fuel cell. The differences in temperature distribution are also very small.

4. Conclusions

The effects of the reformer in the internal-reforming MCFC have been studied by mathematical modeling. The temperature distribution, the conversion of methane and the composition of gases are analyzed through mathematical modeling of the reformer and the cell.

In the reformer, the methane-reforming reaction and the water-gas shift reaction occur simultaneously and the endothermic-reforming reaction contributes to a uniform temperature distribution. The flow rate increases as the reactions proceed. Most of the methane converts to hydrogen under the conditions studied.

The reactants change rapidly at the entrance due to a temperature rise. Hence, the rate of the methane-reforming reaction increases. The equilibrium constant of the water-gas shift reaction becomes small at a high temperature. As a result, the rate of the methane-reaction increases quite slowly due to the water-gas shift reaction.

As the current density increases, the cell voltage decreases and the power increases. On changing the ratio of the fraction of methane to that of water-gas, the largest value of the working voltage is obtained when the ratio is 1:2.

When the conditions of the entering anode gas in the ER-fuel cell are matched with those of the exiting gas from the reformer in the internal-reformimg fuel cell, voltages and current densities in the internal-reforming fuel cell are slightly higher than those in the external-reforming fuel cell.

Acknowledgements

This work was supported by the New & Renewable Energy Program. The authors acknowledge the financial support from the Ministry of Trade, Industry and Energy through R&D Management Center for Energy and Resources and Korea Electro Power Research Institute (KEPRI).

References

[1] Y.J. Ahn, Studies on the cell performance and temperature distributions from mass and energy balances in the molten carbonate unit fuel cell, Master thesis, Hong-ik University, 1994.
[2] T. Shinoki, M. Matsumura, A. Sasaki, IEEE Trans. Energy Convers. 10 (4) (1995) 722.
[3] He Wei, Dynamic Simulations of Molten Carbonate Fuel-Cell System, Delft University Press, Delft, 2000, p. 41.
[4] S.D. Lee, I.C. Hwang, B.G. Lee, I.S. Seo, T.H. Lim, S.A. Hong, Hwahak Konghak 38 (5) (2000) 719.
[5] Y.S. Ahn, G.Y. Chung, J.B. Ju, S.W. Nam, I.H. Oh, T.H. Lim, S.A. Hong, Hwahak Konghak 33 (4) (1995) 479.
[6] P. Muenster, H.J. Grabke, J. Catal. 72 (1981) 279.
[7] J.M. Leo, J. Bolmen, M.N. Mugerwa, Fuel Cell Systems, Plenum Press, New York, 1992, p. 345.
[8] A.J. Appleby, F.R. Foulkes, Fuel Cell Handbook, Krieger Publishing Company, Malabar, FL, 1989, p. 544.
[9] J.R. Selman, Molten Salt Committee of the Electrochemical Society of Japan, 1988.
[10] T.L. Wolf, G. Wilemski, J. Electrochem. Soc. 130 (1) (1983) 48.
[11] J.M. Smith, H.C. van Ness, Introduction to Chemical Engineering Thermodynamics, McGraw-Hill, New York, 1987, p. 482.